A&A 386, 699–708 (2002)
DOI: 10.1051/0004-6361:20020305

Astronomy & Astrophysics

Evidence for weak MHD turbulence in the middle magnetosphere of Jupiter

J. Saur[1,⋆], H. Politano[1], A. Pouquet[2], and W. H. Matthaeus[3]

[1] Laboratoire CNRS CASSINI, Observatoire de la Côte d'Azur, 06304 Nice, France
e-mail: saur@jhu.edu; politano@obs-nice.fr
[2] NCAR/ASP/GTP, Boulder, CO 80303-7000, USA
e-mail: pouquet@ucar.edu
[3] Bartol Research Institute, Newark, DE, USA
e-mail: yswhm@bartol.udel.edu

Received 25 June 2001 / Accepted 17 December 2001

Abstract. In this paper we study the small scale-magnetic field fluctuations of the middle Jovian magnetosphere that are embedded in the strong background field $\boldsymbol{B}_0$ of Jupiter in the framework of turbulence theory. We perform a statistical analysis of these fluctuations using a five year set of Galileo spacecraft magnetic field data. Calculating power spectra of the fluctuations, we identify for the first time a spectral index of minus two for wave vectors perpendicular to $\boldsymbol{B}_0$. These results strongly support a description of the fluctuations within the framework of weak magnetic turbulence and recent theoretical developments therein by Galtier et al. (2000). In addition, we show that there is little variation of the spectral index upon radial distance in the middle magnetosphere. We comment also on how the presence of such fluctuating fields might have interesting consequences concerning transport properties in the Jovian magnetosphere.

Key words. turbulence – MHD – planets and satellites: individual: Jupiter

1. Introduction

The strong magnetic field of Jupiter creates the largest planetary magnetosphere in our solar system. The data gathered from the Galileo spacecraft orbiting Jupiter since December 1995 thus provides a unique possibility to study a wealth of phenomena in this complex environment. In our paper, we investigate the small-scale Jovian magnetospheric fields and describe them in terms of turbulent fluctuations. The results then allow us to discriminate between several competing theories for isotropic and anisotropic configurations of MHD turbulence.

An analysis of the small-scale fluctuations in the Jovian magnetosphere, together with snapshots of their power spectra, have already been presented in Russell et al. (1998, 2000). In their papers, the main thrust is on determining how the amplitude of these fluctuations depends on different locations in the Jovian magnetosphere. In contrast, we now interpret these fluctuations in terms of turbulence. We will examine several theories and models, for both weak and strong MHD turbulence, that have been developed in the context of incompressible flows having constant density ρ and solenoidal plasma velocity $\nabla\cdot\boldsymbol{v} = 0$ (see discussion at the end of this section). Note that the term incompressible refers here to the flow and not to the magnetic field as in Russell et al. (1998, 2000). Such approaches make predictions (in the absence of intermittency), in particular concerning spectral indices, and we shall investigate in detail the slopes of such spectra and discuss their implications. Note that the effect of intermittency, i.e. of the intense localized small–scale structures, can be incorporated as well in such modeling of turbulent flows (see for the MHD case, Politano & Pouquet 1995); at the second–order (energy) level of correlation and structure functions, however, the difference between such intermittent and non–intermittent models are too small to be easily measurable, and will not be considered further in this paper.

Turbulence remains an unsolved problem of classical physics, the difficulty stemming from the presence of nonlinear terms; in incompressible MHD, they are the advection by the velocity field, the Lorentz force and Ohm's law. In the case of stochastic fields, one has to write governing equations for the hierarchy of correlation functions

Send offprint requests to: J. Saur,
e-mail: saur@jhu.edu
⋆ Now at: Department of Earth and Planetary Sciences, Johns Hopkins University, Baltimore, MD, USA.

Table 1. Summary of discussed turbulence theories and phenomenological models; α is the respective spectral index; all are anisotropic except K41 and IK (see comments), $^{(*)}$ see text.

Abbreviation	Authors	α	comments
K41	Kolmogorov (1941)	$-5/3$	model, isotropic, hydrodynamics
IK	Iroshnikov (1963), Kraichnan (1965)	$-3/2$	model, locally isotropic, MHD
SG	Sridhar & Goldreich (1994)	$-7/3$	theory, weak MHD with 4-wave interactions
	Ng & Bhattacharjee (1997)	-2	model, weak MHD with 3–wave interactions
	Goldreich & Sridhar (1997)	-2	model, intermediate MHD with 3-wave interactions$^{(*)}$
G00	Galtier et al. (2000)	-2	theory, weak MHD with 3-wave interactions

of the basic fields, equations that are not closed because of the nonlinearity of the underlying fundamental physics: the equation for the energy (second-order) involves third–order moments, and so on. This is the celebrated closure problem for strong turbulence. Strong turbulence refers to the case when those nonlinear terms are strong – compared to the linear terms that are either dissipative (viscous and resistive) or dispersive (leading in MHD to Alfvén waves growing from unavoidable small perturbations). Such turbulent flows are, at least to a first approximation, considered isotropic, the many waves and eddies in interactions bringing back the symmetries of the problem at small scale even when such symmetries are broken at large scale. Weak turbulence, on the other hand, arises in the presence of a strong uniform external field $\boldsymbol{B}_0$ that allows for a linearization of the MHD equations, and leads one to consider the MHD fluid as a bath of weakly interacting Alfvén waves (and magnetosonic waves in the compressible case); the closure problem can actually be solved in that weak case.

In the absence of a theory for strong turbulence, phenomenology plays an essential role. Assuming self–similarity, the classical evaluation in hydrodynamic turbulence, based on dimensional analysis, leads to a prediction for the energy spectrum $P(k) \propto k^{-5/3}$, where k is the isotropic wavenumber (Kolmogorov 1941, heretofore, K41). Where in Fourier space this spectrum prevails is by definition the "inertial" range. An extension of this phenomenological argument taking into account the presence of Alfvén waves leads on the other hand to $P(k) \propto k^{-3/2}$ (Iroshnikov 1963; Kraichnan 1965, heretofore, IK). For clarity, Table 1 gives a brief summary of the turbulence models considered in this work. Second–order closures of MHD turbulence dealing with the temporal evolution of energy spectra for MHD and incorporating the Alfvén time in a model of eddy–damping are in agreement with the IK prediction (see Pouquet et al. 1976 for the three–dimensional case, and Pouquet 1978 in two dimensions); a new anisotropic closure has also been derived recently in the context of interstellar turbulence (Nakayama 1999) that is also consistent with a 3/2 law.

These are the simplest possible theoretical energy spectra, since they take into account the presence of neither intermittent structures, nor of a strong uniform background magnetic field $\boldsymbol{B}_0$. Indeed, for velocity and magnetic fluctuations embedded within such a field, significant anisotropy linked to the presence of a preferred direction is expected (e.g, Lehnert 1955; Oughton et al. 1994; Matthaeus et al. 1998). Note that the K41 spectrum is advocated as well for strong anisotropic MHD turbulence in Goldreich & Sridhar (1994) in the context of a phenomenological model.

The presence of $\boldsymbol{B}_0$ induces Alfvén waves of wave vectors $\boldsymbol{k}$ and frequencies $\omega(\boldsymbol{k}) = \boldsymbol{k} \cdot \boldsymbol{v}_\mathrm{A}$; the characteristic time of such waves (i.e., the Alfvén time τ_A) becomes in the limit of strong $\boldsymbol{B}_0$ shorter than any other relevant time scale in the problem (e.g. the nonlinear time τ_NL). It thus provides a small parameter

$$\epsilon = \tau_\mathrm{A}/\tau_\mathrm{NL} \tag{1}$$

in which to expand the governing equations (see Table 2 for explicit definitions of τ_A and τ_NL). Together with the resonance conditions between $N = 3$ interacting Alfvén waves, namely

$$\boldsymbol{k}_1 = \boldsymbol{k}_2 + \boldsymbol{k}_3, \quad \omega_1 = \omega_2 + \omega_3, \tag{2}$$

or $N = 4$ interacting waves

$$\boldsymbol{k}_1 + \boldsymbol{k}_2 = \boldsymbol{k}_3 + \boldsymbol{k}_4, \quad \omega_1 + \omega_2 = \omega_3 + \omega_4, \tag{3}$$

this procures natural closures to the successive hierarchy of moment equations of the basic velocity and magnetic fields. Three–wave and four–wave interactions correspond to the two lowest orders in an expansion of the nonlinear terms for strong $\boldsymbol{B}_0$. (See also Newell et al. (2001) for a recent introduction to the weak turbulence regime, and Nazarenko et al. (2001) for a discussion of weak MHD turbulence modeled with non-local interactions.)

Thus in that limit of weak wave turbulence, several analytical results have been derived from the kinetic equations obtained from the closure at second order. In particular, such theories predict an energy spectrum of the form

$$P(\boldsymbol{k}) = F(\boldsymbol{k}_\parallel)\ |\boldsymbol{k}_\perp|^{-\alpha} \tag{4}$$

where $F(\boldsymbol{k}_\parallel)$ is non-universal, $\boldsymbol{k}_\parallel$ is the wave vector parallel to the background field, and $\boldsymbol{k}_\perp$ the wave vector perpendicular to the background field.

Such theories differ by the elementary building blocks they capture, namely either three resonant Alfvén waves,

Table 2. Typical properties of the middle Jovian magnetosphere at the inner Io boundary and outer Callisto boundary. [1] from Neubauer (1998); [2] from Frank et al. (1996); [3] from McNutt et al. (1979). The other variables are estimated from the actual data which we use or are calculated: [4] with $\delta v_A = (\delta b/B_0)v_A$, [5] with $\tau_c = R(0)^{-1}\int_0^\infty d\tau R(\tau)$ with the autocorrelation function $R(\tau)$ (further analyses concerning the calculations based on the increments of the time series $B(t)$ will be presented in Saur et al. in preparation).

	Io	Callisto
Distance from Jupiter r in R_J	5.9	26.4
Background magnetic field[1] B_0 in nT	1835	35
bulk velocity[2,3] v_{bulk} in km s^{-1}	63	200
electron density[1] in cm^{-3}	3600	1.1
plasma beta[1]	0.04	0.18
Alfvén velocity[1] v_A in km s^{-1}	150	188
Sound speed[1] in km s^{-1}	27	73
magnetic fluctuations δb in nT	15	5
$\delta b/B_0$	0.008	0.14
fluctuations in Alfvén vel.[4] δv_A in km s^{-1}	1.2	27
δv_A / v_{bulk}	0.02	0.13
$M = \delta v_A/c_s$	0.04	0.37
Correlation time[5] τ_c in s	600	600
nonlin. time scale $\tau_{NL} = \tau_c v_{bulk}/\delta v_A$ in s	31 000	4500
Alfvén time $\tau_A \approx 4R_J/v_A$ in s	2000	1500
$\epsilon = \tau_A/\tau_{NL}$	0.06	0.34

or four such resonant waves. In Galtier et al. (2000), henceforth G00, three–wave interactions are considered to prevail, leading to $\alpha = 2$. Waves refer here, in the simplest case, to shear Alfvén waves (Galtier et al. 2002). Such a spectral index has also been derived by Ng & Bhattacharjee (1997) and Goldreich & Sridhar (1997) using a straightforward extension of the isotropic IK phenomenology to the anisotropic case. Note that the latter authors call MHD turbulence in that case "intermediate" since they consider that the only exact closure for weak MHD turbulence occurs for 4-wave interactions. Indeed, this $\alpha = 2$ evaluation is in contrast with the theoretical prediction of Sridhar & Goldreich (1994) who obtained the closure equations for weak MHD turbulence in the case where four-wave interactions are the dominant process of energy transfer among scales, leading now to $P(k) \propto k_\perp^{-7/3}$ (henceforth, GS).

In this paper we examine the fluctuations in Jupiter's middle magnetosphere in terms of the above-described turbulent models and theories. We study the fluctuations between the orbits of Io and Callisto, which we call here simply the "middle magnetosphere". Typical parameters found in the middle Jovian magnetosphere are listed in Table 2. Due to Jupiter's strong background magnetic field, the ratio of the magnitude of fluctuating fields to the background field $\delta b/B_0$ are small compared to unity, a fact that favors conditions for weak MHD turbulence. In contrast, the situation in the solar wind differs from the middle Jovian magnetosphere in several interesting ways. The solar wind fluctuations are often of the order of the background field itself, and therefore one might not expect weak MHD turbulence to be relevant. Indeed, spectra with indices close to 5/3, i.e. close to the Kolmogorov value, have been reported, for example, analyzing Voyager data (Matthaeus et al. 1982). On the other hand, some data may also be compatible with the IK spectrum, as measured by the Ulysses spacecraft (Ruzmaikin et al. 1995), especially if one takes into account the effect of steepening due to strong localized intermittent structures (Gomez et al. 1999). Another possibly important distinction, which will be discussed further below, is that the Jovian magnetic field provides a constraint on the long wavelength dynamics of the fluctuations that may have consequences for the types of nonlinear cascades that are possible.

With regard to the relevance of incompressible MHD models, we note that Jovian magnetospheric parameters appear in some ways to be more favorable than for the Solar Wind (see Table 2). For example, in the part of the Jovian magnetosphere where we perform our investigation, the plasma β (ratio of gas to magnetic pressure) ranges from $\beta = 0.04$ to 0.18. In the same region one typically finds small fluctuations δb compared to the local mean field B_0; values of $\delta b/B_0$ in the range of 0.14 to 0.008 are commonplace. A small value of β together with small $\delta b/B_0$ favors incompressibility as a leading order description of low frequency (MHD) plasma dynamics. This can be seen, e.g., in a more formal derivation of incompressibility as a leading order description that makes use of a small turbulent Mach number (M) to develop a nearly incompressible representation (Zank & Matthaeus 1993; Bhattacharjee et al. 1998). ($M = \delta v_A/c_s$, δv_A the fluctuation amplitude in Alfvén speed units and c_s the sound speed.) In the relevant parts of the Jovian magnetosphere, M usually lies in the range 1/25 to ca. 1/3. These parameters are reasonably favorable for a leading order incompressible description. One should note that, in contrast, typical solar wind conditions at 1 AU are $\beta = 1$, $\delta b/B_0 \approx 1$ and $M = 1/3$. Cascade and turbulence theories developed for the incompressible case have found extensive applications in the solar wind context, e.g. Tu & Marsch (1995); Goldstein et al. (1995).

This analysis motivates us to adopt incompressibility as a first working hypothesis, and we neglect compressibility effects in the following considerations. The effect of compressibility, and hence of the coupling of fast and slow magnetosonic waves together with Alfvén waves, is neglected in the theoretical approach predicting a –2 spectrum; a preliminary analysis of the resonant manifolds indicates that energy transfer in the parallel direction is now expected (Galtier et al. 2001), but the full derivation of the kinetic equations remains to be performed.

We thus study in this work the Jovian magnetosphere in terms of spectra for perpendicular and parallel wave vectors in an attempt to discriminate between the available theories, as summarized in Table 1. We first describe the data analysis procedure in Sect. 2, then in Sect. 3

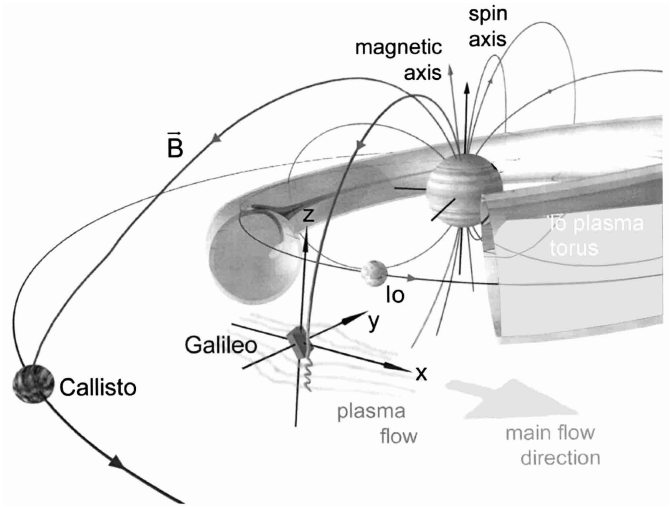

Fig. 1. Geometry of observational setup in the middle Jovian magnetosphere where Jupiter is at center right. Note that the Io plasma torus is displayed in a highly idealized fashion. The plasma of the Jovian magnetosphere actually extends further outwards from the Io torus but is mainly confined to the equatorial region of the magnetosphere. Note also that the Jovian magnetic field axis is inclined by 10 degrees with respect to its spin axis.

we derive the main results. The issue of how weak is the turbulence in the Jovian magnetosphere is addressed in the concluding section (see also Table 2), together with a discussion of the results.

2. Data analysis

We use the magnetic field measurements of the Galileo spacecraft for the years 1995 to 1999, which we have received from the Planetary Data System. Since high resolution measurements are very scarce, because of Galileo's antenna problem, we consider the data set which provides the largest temporal coverage, called the BROWSE data, that are magnetic field data mostly averaged over 12 or 24 s. We did not use the data of orbit C03 (for nomenclature see e.g. Russell et al. 2000) since the data that we have received had been smoothed for technical reasons by a two minute averaging window (M. Kivelson, private communication).

We restrict ourselves to the middle magnetosphere between the orbits of Io and Callisto, i.e., between 6 and 26 R_J, with the radius of Jupiter $R_\mathrm{J} = 71\,400$ km (for the observational setup see Fig. 1). We chose not to use data for the whole magnetosphere in order not to mix up several different effects that take place in the Jovian magnetosphere in significantly different regions, such as regions with open field lines configurations. With this choice, we also ensure that the magnitude of the fluctuations are small compared to the background magnetic field, which is the parameter regime where we want to perform our analysis.

For our analysis window between 6 and 26 R_J, the bulk velocity v_bulk of the magnetospheric plasma ranges from 63 km s^{-1} near Io to $v_\mathrm{bulk} = 200$ km s^{-1} at Callisto (i.e. close to Io, the plasma is in nearly full corotation while at Callisto the deviations are already about 40%). Referring to Table 2, we see that v_bulk is expected to be greater than the fluctuation speed δv_A throughout the region of interest. Consequently we can employ the familiar Taylor frozen–in flow assumption that allows time separations to be interpreted as spatial separations, and therefore frequency spectra to be interpreted as reduced wavenumber spectra. This approximation is used in a number of applications, such as for the solar wind (e.g., Jokipii 1973; Matthaeus & Goldstein 1982).

We divide the whole data set in blocks of length one hour in order to analyze only the magnetospheric components of the signal that have periods short compared to Jupiter's rotation period of ten hours. This choice of interval length is also intended to allow a stable estimate of the local mean magnetic field in each 1 hour bin. For the periodically varying background field, this corresponds to dividing one period of a sinusoidal field into 10 averaged subsets. It thereby enables us also, to distinguish effects due to different projections on the changing background magnetic field. In addition, the one hour period separates intervals according to whether they are in or out of the Jovian centrifugal equator. The choice of interval length is a compromise between staying clearly under the 10 hour rotation period of Jupiter, which determines the background field, and a need to have sufficient data in each block to calculate meaningful power spectra.

In addition, we search the one hour data blocks out of the full data set so that the maximum data gap in each block is less than or equal to 24 s. With this procedure we find a total of 1066 one hour blocks. We then interpolate the data within each block on an equidistant grid with 257 points, i.e. to a temporal resolution of 14 s.

In each block, we work with a local coordinate system and thus rotate the data in such a way that the z-axis is anti-parallel to the local background magnetic field $\boldsymbol{B}_0$, and thus points mostly northward. $\boldsymbol{B}_0$ is calculated from the average measured field within each 1 hour block. We choose the x-axis to be in the plane given by the background field and the direction of rotation of the spin equator. The y-axis completes the right-handed coordinate system. Finally, we remove the background magnetic field and its trend calculated from the actual data. We then use the method of increments, i.e. we work with the time series $\Delta B(t_{n+1}) = B(t_{n+1}) - B(t_n)$ (see Bieber et al. 1993) to remove non-stationary elements out of the data (see two paragraphs below). This is essentially equivalent to prewhitening the data and then postdarkening after the spectral analysis. Finally we calculate the power spectra for each magnetic field component using the Fast-Fourier-Transformation in a frequency range $f_0 = 2.78 \times 10^{-4}$ Hz to 3.57×10^{-2} Hz following the conventions in Bendat & Piersol (1971).

Since the magnetic field data in the Jovian magnetosphere sometimes exhibit jumps, which are thought to be due to the interchange instability (e.g., Kivelson et al. 1997), we took into consideration only data blocks where the difference in the preprocessed data from one point to another was at most 0.7 nT in order to remove the possible impact of these jumps on the turbulence power (e.g., Roberts & Goldstein 1987). In this way we used for our analysis 221 blocks of length one hour.

Another data analysis issue pertains to estimates of the stationarity of samples, e.g. Matthaeus & Goldstein (1982). The concern is that the selection of data might bias the sample (or, "ensemble") to which the spectral analysis is applied. In the case of the Solar Wind, the conclusion derived from such considerations has usually been that data samples should be short compared to the solar rotation period (27 days) and long compared to the correlation time (see Table 2 for definition). Here the Jovian rotation period of 10 hours is more constraining, forcing smaller analysis blocks. To investigate whether this provides a reasonable ensemble from which to proceed, we carried out a quantitative study (not shown) of convergence of estimates of local mean values to stable values. The procedure was tested against artificial data (see e.g., Saur et al., in preparation). We found that the convergence of our estimates can be understood by modeling the signal as a stationary random process, plus long period oscillations that are under-sampled, including the Jovian rotation. It is interesting that the problem with undersampling affects mostly the estimates of the means, while estimates of the variances behave as expected from theoretical considerations (Matthaeus & Goldstein 1982). Although a technical point, this test of the method has given us confidence that we understand the behavior of the data set. On this basis we believe our spectral analysis to be well justified.

Our available set of magnetic field data also contains periodic signatures which are due to the spin of the Galileo spacecraft. The spin period of the Galileo spacecraft varies closely around 19 s (M. Kivelson, private communication). From the BROWSE data set, which we analyze, we only take subintervals where the sampling rate is less than or equal to 24 s. The most prominent sampling rates in these subsets are 24 and 12 s which undersample the spin period and create artificial aliased frequencies at 0.031 Hz and 0.011 Hz, respectively. A fraction of the data is sampled at less than 19/2 s which does not cause a problem. In our analysis we interpolate the data on an equidistant grid of 14 s leading also to an aliased frequency at 0.019 Hz. This aliasing produces artificial power which is not part of the Jovian magnetospheric processes. In our interpretation of the physics of the fluctuations we therefore consider only frequencies which are smaller than 0.011 Hz where we do not expect artificial power due to the spacecraft spin.

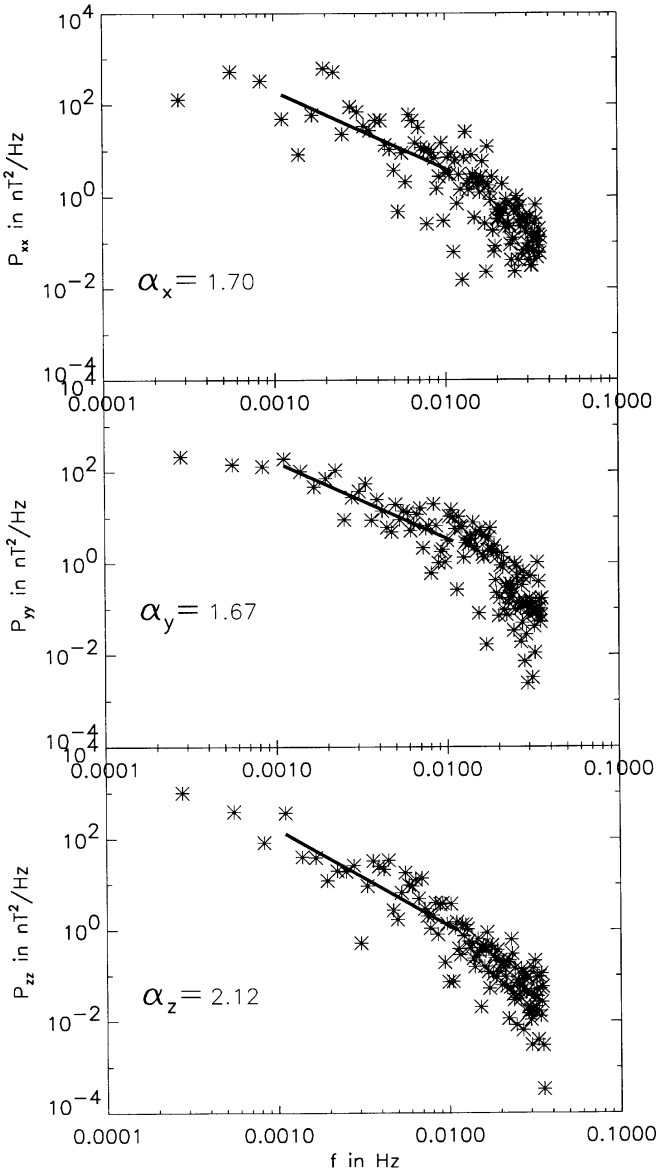

Fig. 2. Example of individual spectra and their fitted power laws for all three magnetic field components, for a typical one–hour subset of the data.

3. Measurements

3.1. Examples of spectra

In Fig. 2, we show a typical example of three spectra for a one hour block data sample. The asterisks display the calculated power spectra and the solid lines refer to a power law fit of the form $P_{ii} = P_{ii,0}(f/f_{\rm p})^{\alpha_i}$, with α_i indicated in each case. We denote as P_{ii} the power spectrum of the fluctuations δb_i in direction i, with $i = x, y$, or z and $P_{ii,0}$ the reference power at a chosen frequency $f_{\rm p}$. This data block is taken from the Galileo spacecraft orbit C22 starting August 13th 1999 at 17:07 UT at an average distance of 20 $R_{\rm J}$. The power laws are fitted in a subset of the available range (see below), and display large scatter in individual blocks, the effect of which is smoothed by averaging over 221 blocks. Note the steeper slope for the

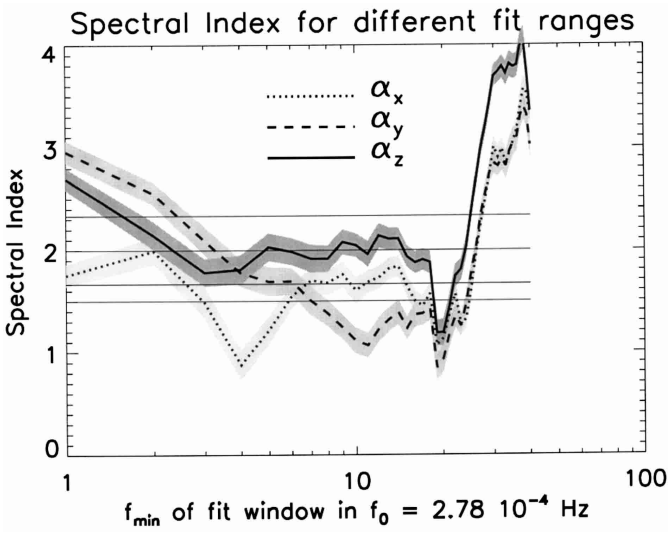

Fig. 3. Determination of the inertial range and its spectral index for each magnetic field component; $f_{\min}$ is the lower corner frequency of the fit window of length one octave and it is measured in units of our lowest available frequency $f_0 = 1/1\,\mathrm{h}$. Error estimates are displayed with the grey shaded regions and are calculated in the standard manner using the calculated values of α in each of the 221 blocks. The horizontal lines represent the various phenomenological or theoretical predictions (see text and Table 1).

parallel component of the spectrum, whereas the perpendicular components have comparable spectral indices.

3.2. Determination of inertial indices

When we fit the calculated power spectra to a meaningful power law, it is first of all necessary to determine the fit range, i.e. we need to find out the inertial range where a self-similar cascade process of energy transport from larger to smaller scales occurs. Therefore we introduce a spectral window of one octave, i.e. $f_{\max}/f_{\min} = 2$ and move that window over our total frequency range and determine in each case the spectral index. Actually we used an octave plus one frequency point, in order to have at the lowest frequency at least three fit-frequencies. Moving the window within the inertial range should result in a constant spectral index.

The results of our search for the inertial range and its spectral index are shown in Fig. 3. We plot the spectral index calculated in each spectral window upon the minimum frequency $f_{\min}$ of each fit window. We will call this frequency the left "corner frequency" of our spectral fit windows. For the fluctuations along the background magnetic field, we find for the power spectrum P_{zz} a relatively constant spectral index α_z of -2 ± 0.1 within the corner frequencies $f_{\min}$ from 5 f_0 to nearly 19 f_0. At frequencies $f_{\min}$ larger than 19 f_0 the spacecraft spin gives an artificial power due to aliasing which does not allow us to draw further conclusions for any higher frequencies (see discussion in Sect. 2). Thus, together with the frequency octave of the fit window we find a frequency range of 1.38×10^{-3} Hz to 1.1×10^{-2} Hz, i.e. about one decade where we get a spectral index of -2 within our error bars. We call this frequency interval the inertial range, as available to us. For the spectral index of the power spectra of the fluctuations in the x and y directions, we do not find an obvious inertial range; consequently, their spectral indices (noted $\alpha_\perp$) have stronger variations in this same range of frequencies, namely $\alpha_\perp = 1.5 \pm 0.3$. The error bars in Fig. 3 are sufficiently small that one can conclude that there is a significant difference between the two sets of indices, parallel and transverse to the magnetic field $\boldsymbol{B}_0$. The horizontal lines in Fig. 3 represent the theoretical predictions of GS (2.33) and G00 (2.0), and the phenomenological evaluations of K41 (1.67) and IK (1.5), as described in the comments of Eq. (4) and Table 1.

3.3. A model to interpret the data

Now we provide an interpretation for the observed spectral index in terms of a binary model of MHD turbulence which is often invoked to explain several features of the Solar Wind (Bieber et al. 1996; Saur & Bieber 1999), in particular the so–called "Maltese cross", which shows that modes with wave vectors parallel or perpendicular to $\boldsymbol{B}_0$ are much more strongly populated than are oblique wave vectors (see Matthaeus et al. 1990). In the framework of such a model, the turbulence results from a combination of a pure slab field $\delta\boldsymbol{b}^{\mathrm{s}}(k_\parallel)$ and a pure two–dimensional field $\delta\boldsymbol{b}^{(2\mathrm{D})}(k_\perp)$.

The slab field has, by definition, only a dependence on the parallel wave vector $k_\parallel$, and hence, from the divergence–free condition, has an identically zero parallel component, $\delta\boldsymbol{b}^{\mathrm{s}}_\parallel(k_\parallel) \equiv 0$. On the other hand, the 2D field has only perpendicular variations but all three components survive. Since we observe substantial power in all three components we assume a mixture of both slab and 2D turbulence for the Jovian fluctuations, similar to the Solar Wind. This allows us to conclude that the *parallel* component of that turbulence can only be 2D and thus shows *only* a $\boldsymbol{k}_\perp$ dependency. Hence, the spectral index for P_{zz} is a $k_\perp^{-2}$ dependency, and its -2 value is as predicted in the weak turbulence theory of Galtier et al. (2000), and the phenomenological approaches of Ng & Bhattacharjee (1997), and Goldreich & Sridhar (1997), all based on three–wave interactions.

Note also that the total power in the projections goes as $\cos(\phi)^{\alpha-1}$ for the slab component and $\sin(\phi)^{\alpha-1}$ for the 2D component (see Bieber et al. 1996), where ϕ is the angle between the velocity and the magnetic field, and α is the afore mentioned spectral index. The main feature of this dependence can be seen from looking, for example, at 2D turbulence. In this case of 2D turbulence one observes for $\phi = 0$ i.e. parallel to the background field where no wave vectors are excited and thus no power can be seen in this projection; on the other hand, for $\phi = 90$, one observes perpendicular to the background magnetic field and thus in the direction of the excited wave vectors for 2D-turbulence where consequently power can be seen

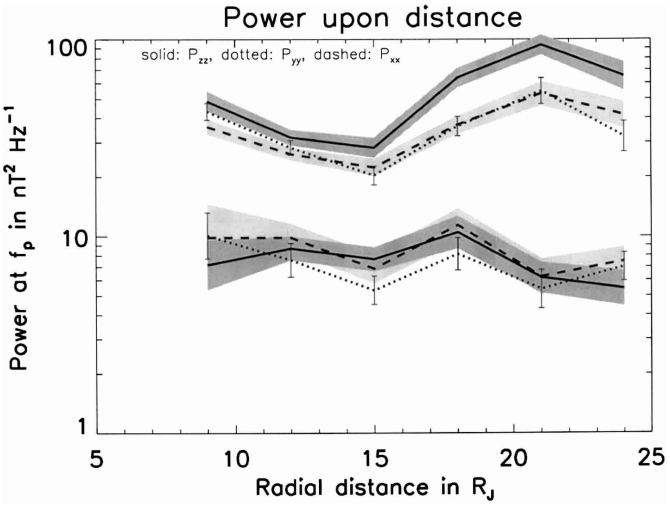

Fig. 4. Variation of power of spectra at frequency 2.4×10^{-3} Hz upon radial distance. Error estimates for P_{zz} and P_{xx} are displayed using grey–shading, and those for P_{yy} with error bars for clarity. The lower three curves are calculated from the jump filtered data (see text), which we also use for the other quantities displayed and discussed in this paper. For completeness we also show the power dependence for the original non jump filtered data in the upper three curves.

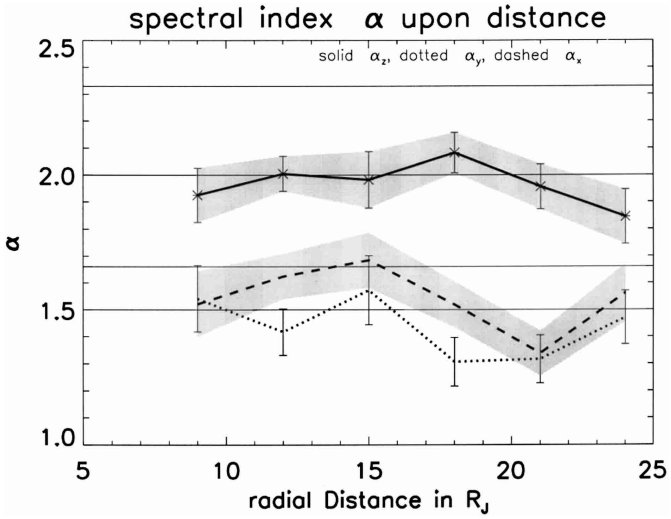

Fig. 5. Variation of spectral index α upon radial distance for each component. Error estimates for α_z are displayed with grey-shading and with standard error bars, errors on α_x are displayed only with grey-shading, while errors on α_y are displayed only with error bars for clarity.

in accordance with the $\sin(\phi)^{\alpha-1}$ dependence. The Jovian background magnetic field is mostly perpendicular to the mean magnetospheric plasma flow, but variations around $\phi = 90$ arise due to the fact that Jupiter's magnetic field moment is inclined by 10 degrees with respect to Jupiter's spin axis. Therefore projection effects also come into play, but we basically have very little access to measure the power that resides in fluctuations with wave vectors parallel to the background magnetic field because of the observational geometry.

The origin of the difference between $\alpha_\perp$ and α_z is an open issue. Indeed, the dependency in the transverse directions differs from that predicted by weak turbulence theory which yields a similar variation with $k_\perp$ for all components of the basic fields. But, as noted before, the unraveling of the $k_\parallel$ and $k_\perp$ variables is only feasible for the parallel spectrum P_{zz} and in the framework of the binary (slab/2D) model. Hence, the P_{xx} and P_{yy} spectra may have a variation with $k_\parallel$, that is not predicted by the weak turbulence formalism (it is non–universal and may reflect some "initial" field properties, for example as advected to where we observe it). We may as well just have poor access to the $k_\parallel$–variation of P_{xx} and P_{yy} because of the observing geometry. This $k_\parallel$ variation may also come from a strong contribution of the slab component to Jovian turbulence, as well as from compressible effects (Galtier et al. 2001). Finally, in numerical simulations of anisotropic MHD turbulence, spectra for the parallel component are observed to be steeper than for the transverse components (Milano et al. 2001), both in the presence of a *dc* field i.e. in the realm of weak MHD turbulence, as well as in the case $\boldsymbol{B}_0 \equiv 0$ (in this case, taking into account the direction of the *local* magnetic field). We also note that the two transverse components of the spectral energy tensor P_{xx} and P_{yy} include contributions from both the poloidal and toroidal fields, as well as from the non–helical part of their cross-correlation (see Galtier et al. 2000), whereas the parallel energy tensor P_{zz} involves only the poloidal part of the fields. This could explain the difference in behavior of the three spectra (see Fig. 3). Further work is needed to decipher this part of the problem.

3.4. Examination of variations with radial distance to Jupiter

We now examine how the power of each component varies with radial distance in the Jovian magnetosphere (Fig. 4) at $f_\mathrm{p} = 2.4 \times 10^{-3}$ Hz. Note that the shaded regions indicate the errors for the x and z components, whereas error bars are directly displayed for the y component, in order that all three curves be easily readable. The same remark applies for Fig. 5, although error bars are also displayed for α_z (see below). Due to our selection of blocks by demanding that the maximum increment be less than 0.7 nT, we have removed also blocks with large fluctuations in general. In this manner, our sub-data set exhibits a relatively constant power upon radial distance as seen in Fig. 4, lower three curves. However if we do not preselect the data with this jump criterion, we then find that the amplitude of the fluctuation upon distance in the middle Jovian magnetosphere does not vary in a way proportional to the strength of the background magnetic field, see upper three curves in Fig. 4. Note that, apart from the three upper curves in Fig. 4, all other results shown and derived in this paper are based on our jump-filtered sub-data set (see Sect. 2). This implies that the relative strength of the weak turbulence fluctuations (i.e. the ratio

of the strength of the fluctuations to the background field) strongly increases with radial distance. This power distribution variation upon radial distance might reflect on the one hand the source distribution of the energy input, and on the other hand the development of turbulence in the magnetosphere.

In Fig. 5 we show how the spectral indices themselves depend upon the radial distance. There is no significant dependence visible. The spectral index α_z stays constant around -2 and the Kolmogorov or IK (5/3 or 3/2) spectral indices, as well the GS estimation of 7/3, all can be excluded clearly, all across the middle magnetosphere for α_z. However for the transverse x and y components, we find consistently lower values for such transverse indices, but their significance is lessened by the fact that the potential inertial range has a smaller span, as displayed in Fig. 3, and because the $\boldsymbol{k}_\parallel$ dependency comes into play as well, as discussed before.

We finally remark that in Galtier et al. (2000), one finds an evaluation of the Kolmogorov constants C_t and C_p of the corresponding spectra for the toroidal (or $\perp$) and poloidal (or $\parallel$) components of the basic fields with respective energy fluxes P_t and P_p:

$$E_\mathrm{t} = C_\mathrm{t} P_\mathrm{t}^{1/2} k_\perp^{-2}; \quad E_\mathrm{p} = C_\mathrm{p} P_\mathrm{p} P_\mathrm{t}^{-1/2} k_\perp^{-2}, \tag{5}$$

so that

$$\frac{E_\mathrm{t}}{E_\mathrm{p}} = \frac{C_\mathrm{t}}{C_\mathrm{p}} \frac{P_\mathrm{t}}{P_\mathrm{p}}. \tag{6}$$

These constants are strikingly different: evaluating their ratio for zero velocity magnetic–field correlations, one finds $C_\mathrm{t}/C_\mathrm{p} \sim 10$ (see Figs. 2 and 4 in Galtier et al. 2000). Now using the observed fact that the ratio of the energy in the parallel and the two transverse components of the power spectra is roughly equal to unity, as indicated in Fig. 4, at the frequency of 2.4×10^{-3} Hz at which this figure is drawn, we can deduce in the framework of the present work that the toroidal flux through the weak turbulence cascade is an order of magnitude weaker than its poloidal counterpart, at that frequency. Similar results hold when the variation of power with distance is examined at a frequency of 1.1×10^{-3} Hz (not shown here); going now to substantially larger frequencies, the ratio between the parallel and transverse powers is more like a factor of three, and thus the poloidal and toroidal fluxes differ now also by a factor three. This seems to hold in fact for any value of the velocity magnetic–field correlation (compare Figs. 2 and 4 in G00).

4. Conclusions

We have shown in this paper that the small-scale magnetic field fluctuations in the middle Jovian magnetosphere can be interpreted in terms of a weak turbulence approach and that their statistical behavior strongly supports the analytical evaluation (Galtier et al. 2000) of a "-2" spectral index for perpendicular wave vectors in weak MHD turbulence embedded within a strong background magnetic field. This observational confirmation of a -2 perpendicular spectrum for a plasma undergoing weak turbulence interactions addresses the fundamental question of the prevalence of three–wave interactions over higher–order processes, such as four–wave interactions, and is the first of its kind.

Since Jupiter possesses a very strong internal magnetic field and thus a gigantic magnetosphere with several strong large scale energy sources within the magnetosphere, it may provide an interesting laboratory to test basic questions of weak MHD turbulence. Two of the main energy sources one might identify are (i) the 10 degree tilt of the Jovian magnetosphere with respect to its spin axis which forces movement of the equatorial plasma within a 10 hour period; and (ii) the radial mass transport due to the strong mass loading of the Galilean satellites, in particular Io (with about 10^3 kg/s) where the mass is transported radially outward in a non–continuous process, called interchange motion (e.g., Kivelson et al. 1997).

Although the spectral index results for the parallel fluctuation component is fairly compelling with regard to the -2 slope and its connection to weak turbulence, there remain issues that warrant further examination with regard to our principal conclusions.

For example, we have argued heuristically for weak turbulence when $\delta b/B_0$ is small, but an equivalent necessary condition (Galtier et al. 2000) is that the Alfvén time scale be shorter than the nonlinear time scale for the fluctuations, for the problem to be a viable candidate for a weak MHD turbulence description. Let us estimate the nonlinear time scale as $\tau_\mathrm{NL} = \lambda_\perp/\delta v_\mathrm{A}$, where $\lambda_\perp$ is the correlation length scale of the turbulence, evaluated here on the correlation time and the (large–scale) bulk velocity of the fluid. In that case, referring to Table 2, we can estimate τ_NL to be 3.1×10^4 s at 5.9 R_J and $\tau_\mathrm{NL} = 4.5 \times 10^3$ s at 26 R_J. These are to be compared with the corresponding Alfvén times τ_A of 2000 s and 1500 s respectively. For estimating the Alfvén times we assumed that the plasma in the equatorial region of the Jovian magnetosphere extends roughly 2 R_J in each direction along the magnetic field lines. The condition $\tau_\mathrm{A} \ll \tau_\mathrm{NL}$ is fulfilled in the middle Jovian magnetosphere, and better so in the inner part of our analysis region. This conclusion, qualitatively, corroborates the remark that $\delta b/B_0 \ll 1$ (in fact, $\delta b/B_0$ and $\epsilon = \tau_\mathrm{A}/\tau_\mathrm{NL}$ are comparable, as expected). So weak turbulence appears to be best justified in the inner region, but still to be valid in the outer region. However, we expect in regions outside of the location we selected, i.e. at some point beyond the orbit of Callisto, that the turbulence starts to leave the weak turbulence regime. Though potentially interesting, we do not address this issue in our current paper where we focus on the weak turbulence region only.

Note however that this breakdown of the weak turbulence regime is known to take place, in a finite time, at small scale for MHD (Newell et al. 2001), and has been advocated as well on a phenomenological basis in

(Goldreich & Sridhar 1997). This breakdown of the approximation stems from the simple fact that the weak turbulence limit is non-uniform in scale. Indeed, the small parameter $\epsilon = \tau_A/\tau_{NL}$ introduced in Eq. (1) is in fact scale–dependent; with an energy spectrum $E(k_\perp) \sim k_\perp^{-2}$, the eddy turn-over time $\tau_{NL} \sim \ell_\perp/v_{\ell_\perp}$ decreases with wavenumber. As the weakly nonlinear cascade proceeds to large wavenumbers, the weak turbulence approximation becomes less justified since the Alfvén time is considered fixed.

Another possible cause for concern is that the transverse power spectra have not been shown to follow the weak turbulence scaling. This has been explained in a preliminary way by appealing to the fact that the parallel spectrum contains no "pollution" by parallel propagating waves, and the latter may have any spectral law whatsoever in highly anisotropic turbulence in which perpendicular cascade dominates. Nevertheless our conclusions would be more secure if there was some hint that the transverse power spectra were influenced by the weak turbulence cascade scenario.

Finally, we would like to comment on an additional reason as to why we are finding a possible signature of weak turbulence in the Jovian magnetosphere, whereas the solar wind typically shows a strong turbulence spectrum. In the present case, the inequality $\tau_A \ll \tau_{NL}$ is supported by the limit that exists on parallel length scales in the Jovian magnetosphere, i.e. the field lines are closed in the middle magnetosphere (see Fig. 1) and thus have finite length. Since the magnetic field strength is large, and there is a maximum wavelength parallel to the field imposed by the magnetospheric geometry, it is difficult for a given B_0 to place much power into the strictly non-propagating ("zero frequency") modes that characterize strong turbulence.

In fact, the opposite inequality, $\tau_{NL} \leq \tau_A$ would be required for validity of a fully low frequency strong turbulence model such as that of Reduced MHD (Strauss 1976; Montgomery 1982; Zank & Matthaeus 1993). In this way the approximations leading to weak turbulence can be seen as naturally mutually exclusive to those leading to zero frequency strong turbulence. In summary, the present observational analysis strongly suggests that weak turbulence is the more likely candidate for application to the middle Jovian magnetosphere.

The observations of weak MHD turbulence in the Jovian magnetosphere, as proposed here, may also have interesting consequences for our understanding of the Jovian magnetosphere itself; indeed, transport processes might be controlled by weak turbulence interactions. For instance, we expect these turbulence processes to set up an anomalous resistivity along the magnetic field lines, which might significantly alter (in fact, weaken) the coupling of the magnetosphere to Jupiter and the transport of torque of Jupiter to maintain corotation (or partial corotation) in the Jovian magnetosphere; it would thus modify the coupling mechanism suggested by Hill (1979, 1980), who assumed infinite conductivity along the magnetic field lines. The small-scale turbulent fluctuations might have also consequences for the diffusion processes of energetic particles in the Jovian magnetosphere. These issues are left for future work.

For future research it might also be interesting to study the long term temporal behavior of the fluctuations in the Jovian magnetosphere. For example, one could look for a potential relationship connected to the activity of Io and the mass loading of the magnetosphere. We finally suggest applying a similar analysis to Saturn's magnetosphere, especially when data of the Cassini spacecraft will become available.

Acknowledgements. We would like to thank Margaret Kivelson and her team for providing us, via PDS, the magnetic field data of the Galileo spacecraft and her and Joe Mafi's very helpful comments on technical issues regarding the data set. Thanks to Christer Neimöck for Fig. 1, and to Sébastien Galtier for useful discussions. This work has been supported in part by the CNRS Programs PCMI and PNST. We also would like to thank the anonymous referee for his/her careful reading and constructive comments on our original manuscript.

References

Bendat, J. S., & Piersol, A. G. 1971, Random Data: Analysis and measurement procedures (Wiley-Interscience)
Bieber, J. W., Chen, J., Matthaeus, W. H., et al. 1993, J. Geophys. Res., 98, 3585
Bieber, J. W., Wanner, W., & Matthaeus, W. H. 1996, J. Geophys. Res., 101, 2511
Bhattacharjee, A., Ng, C. S., & Spangler, S. R. 1998, ApJ, 494, 409
Frank, L. A., Paterson, W. R., Ackerson, K. L., et al. 1996, Science, 274, 394
Galtier, S., Nazarenko, S. V., Newell, A. C., & Pouquet, A. 2000, J. Plasma Phys., 63, 447
Galtier, S., Nazarenko, S. V., & Newell, A. C. 2001, Nonlinear Proc. in Geophys., 8, 141
Galtier, S., Nazarenko, S. V., Newell, A. C., & Pouquet, A. 2002, ApJ, 564, L49
Goldreich, P., & Sridhar, S. 1994, ApJ, 438, 763
Goldreich, P., & Sridhar, S. 1997, ApJ, 485, 680
Goldstein, M. L. S., Roberts, D. A., & Matthaeus, W. H. 1995, ARA&A, 33, 283
Gomez, T., Politano, H., & Pouquet, A. 1999, Phys. Fluids, 11, 2298
Hill, T. W. 1979, J. Geophys. Res., 84, 6554
Hill, T. W. 1980, Science, 207, 301
Iroshnikov, P. 1963, Sov. Astron., 7, 556
Jokipii, J. R. 1973, RA&A, 11, 1
Kivelson, M. G., Khurana, K. K., Russell, C. T., & Walker, R. J. 1997, Geophys. Res. Lett., 24, 2127
Kolmogorov, A. N. 1941, Dokl. Akad. Nauk. SSSR, 30, 9
Kraichnan, R. H. 1965, Phys. Fluids, 8, 1385
Lehnert, B. 1955, Quart. Appl. Math., 12, 321
McNutt, R. L., Belcher, J. W., Sullivan, J. D., Bagenal, F., & Bridge, H. S. 1979, Nature, 280, 803
Matthaeus, W. H., & Goldstein, M. L. 1982, J. Geophys. Res., 87, 6011
Matthaeus, W. H., & Goldstein, M. L. 1982, J. Geophys. Res., 87, 347
Matthaeus, W. H., Goldstein, M. L., & Roberts, D. A. 1990, J. Geophys. Res., 95, 20 673

Matthaeus, W. H., Oughton, S., Ghosh, S., & Hossain, M. 1998, Phys. Rev. Lett., 81, 2056
Milano, L. J., Matthaeus, W. H., Dmitruk, P., & Montgomery, D. C. 2001, Phys. Plasmas, 8, 2673
Montgomery, D. 1982, Phys. Scr., T2/1, 83
Nakayama, K. 1999, ApJ, 523, 315
Newell, A. C., Nazarenko, A. C., Biven, S., & Physica, D. L. 2001, 152–153, 520
Ng, C. S., & Bhattacharjee, A. 1997, Phys. Plasmas, 4, 605
Neubauer, F. M. 1998, J. Geophys. Res., 103, 19 844
Oughton, S., Priest, E. R., & Matthaeus, W. H. 1994, J. Fluid Mech., 280, 95
Politano, H., & Pouquet, A. 1995, Phys. Rev. E, 52, 636
Pouquet, A., Frisch, U., & Léorat, J. 1976, J. Fluid Mech., 77, 321
Pouquet, A. 1978, J. Fluid Mech., 88, 1
Roberts, D. A., & Goldstein, M. L. 1987, J. Geophys. Res., 92, 10 105
Russell, C. T., Huddleston, D. E., Khurana, K. K., & Kivelson, M. G. 1998, Planet. Space Sci., 47, 133
Russell, C. T., Huddleston, D. E., Khurana, K. K., & Kivelson, M. G. 2000, Adv. Space Res., 26, 1489
Ruzmaikin, A., Feynman, J., Goldstein, B. E., Smith, E. J., & Balogh, A. 1995, J. Geophys. Res., 100, 3395
Saur, J., & Bieber, J. W. 1999, J. Geophs. Res., 104, 9975
Strauss, H. R. 1976, Phys. Fluids, 19, 134
Sridhar, S., & Goldreich, P. 1994, ApJ, 432, 612
Tu, C.-Y., & Marsch, E. 1990, J. Geophys. Res, 95, 4337
Tu, C.-Y., & Marsch, E. 1995, Space Sci. Rev., 73, 1
Zank, G. P., & Matthaeus, W. H. 1993, Phys. Fluids, 5, 257